ADVANCED MATERIALS
www.advmat.de

Volumetric Bioprinting of Complex Living-Tissue Constructs within Seconds

Paulina Nuñez Bernal, Paul Delrot, Damien Loterie, Yang Li, Jos Malda, Christophe Moser, and Riccardo Levato**

Biofabrication technologies, including stereolithography and extrusion-based printing, are revolutionizing the creation of complex engineered tissues. The current paradigm in bioprinting relies on the additive layer-by-layer deposition and assembly of repetitive building blocks, typically cell-laden hydrogel fibers or voxels, single cells, or cellular aggregates. The scalability of these additive manufacturing technologies is limited by their printing velocity, as lengthy biofabrication processes impair cell functionality. Overcoming such limitations, the volumetric bioprinting of clinically relevant sized, anatomically shaped constructs, in a time frame ranging from seconds to tens of seconds is described. An optical-tomography-inspired printing approach, based on visible light projection, is developed to generate cell-laden tissue constructs with high viability (>85%) from gelatin-based photoresponsive hydrogels. Free-form architectures, difficult to reproduce with conventional printing, are obtained, including anatomically correct trabecular bone models with embedded angiogenic sprouts and meniscal grafts. The latter undergoes maturation in vitro as the bioprinted chondroprogenitor cells synthesize neo-fibrocartilage matrix. Moreover, free-floating structures are generated, as demonstrated by printing functional hydrogel-based ball-and-cage fluidic valves. Volumetric bioprinting permits the creation of geometrically complex, centimeter-scale constructs at an unprecedented printing velocity, opening new avenues for upscaling the production of hydrogel-based constructs and for their application in tissue engineering, regenerative medicine, and soft robotics.

P. N. Bernal, Dr. Y. Li, Prof. J. Malda, Dr. R. Levato
Department of Orthopaedics
University Medical Center Utrecht
Utrecht University
3584CX Utrecht, The Netherlands
E-mail: r.levato-2@umcutrecht.nl

Dr. P. Delrot, Dr. D. Loterie, Prof. C. Moser
Laboratory of Applied Photonics Devices
École Polytechnique Fédéral Lausanne (EPFL)
CH-1015 Lausanne, Switzerland
E-mail: christophe.moser@epfl.ch

Prof. J. Malda, Dr. R. Levato
Department of Equine Sciences
Faculty of Veterinary Medicine
Utrecht University
3584CX Utrecht, The Netherlands

The ORCID identification number(s) for the author(s) of this article can be found under https://doi.org/10.1002/adma.201904209.

DOI: 10.1002/adma.201904209

Living tissues owe their functionality predominantly to their complex architecture. The topographical and geometrical cues provided by the extracellular milieu, together with the precise and anisotropic spatial distribution of morphogens and biochemical signals, are well recognized as major determinants of cell fate both in vitro and in vivo.[1–4] Capturing such a shape–function relationship within engineered biomaterials holds great potential for the creation of new cell-instructive implants that can unlock the regenerative potential of embedded or recruited cells upon grafting in situ. Irregular and anisotropic architectures are fundamental, for example, in the load-bearing function of cancellous bone as the trabecular framework aligns along the main direction of stress,[5] in the shock-absorber function of menisci, where geometry and zonal architecture distribute applied loads,[6] or in the contractile function of cardiac and skeletal muscle, as cell alignment provides directionality for force generation.[7]

Biofabrication technologies are emerging as powerful tools to drive tissue regeneration. This is owed to their ability to accurately control the spatial orchestration of multiple cell types and biomaterials in an automated patterning process.[8,9] Although this discipline is still in its early stages of development, the presentation of optimized geometrical features and biomimetic architectures within biofabricated constructs has shown remarkable achievements in the restoration of salient tissue functions even in vivo, for instance, within biofabricated ovaries[10] and thyroid glands.[11]

Despite such promising advances, new developments are necessary to enable the creation of large, clinically relevant biofabricated grafts, with potential application for regenerative medicine in humans, produced with a high-speed scalable process. Current (bio)printing and additive manufacturing methods include extrusion-based techniques, lithographic printing, that is, stereolithography (SLA) and digital light projection printing employing digital micromirror devices (DLP/DMD), laser-based methods, and melt electrowriting. These all build 3D objects in a layer-by-layer fashion, typically patterning voxels or extruded fibers as essential building units.[8] This feature greatly limits the type of structures that can be generated, which often require supports to produce the complex hollow features and overhangs, typical of biological

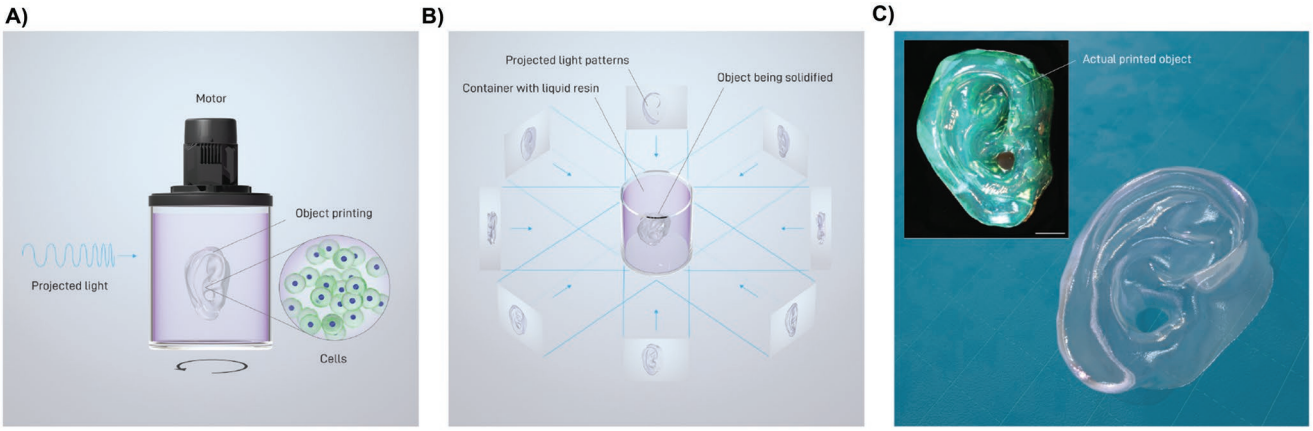

Figure 1. Overview of the volumetric bioprinting process, showing A) the cell-laden gelRESIN reservoir connected to a rotating platform, B) a schematic of tomographic projections used to print the human auricle model, and C) a rendering of the resulting printed hydrogel structure. The inset in (C) shows a stereomicrograph of the actual printed hydrogel, stained with alcian blue to facilitate visualization (printing time = 22.7 s; scale bar = 2 mm).

structures (i.e., due to intrinsic porosity and the presence of vasculature). Importantly, these printing processes take considerable time, especially when large, centimeter-scale grafts need to be generated.[8] Such extended fabrication times impose the requirement to keep the cells in a printer cartridge or within a printed construct outside an optimal culture environment for long periods. This can cause significant stress to cells and substantially impair their functionality.[12,13] This issue becomes even more significant when larger constructs are generated with high-resolution printing methods, such as those involving coprinting of microfibers and cells[12] or two-photon polymerization.[14] Thus, overcoming these limitations of layer-by-layer additive manufacturing in the field of tissue biofabrication is of great interest to open new avenues toward the successful generation of larger, clinically relevant engineered constructs.

Volumetric printing technologies introduce a paradigm shift, as they enable the creation of entire objects at once, rather than through the sequential addition of basic building blocks. In this study, the concept of volumetric bioprinting (VBP) is introduced, enabling the fabrication of entire cell-laden constructs with arbitrary size and architecture within a time frame of seconds to tens of seconds. As recently implemented, volumetric additive manufacturing relies on the projection of a series of 2D patterned optical light fields within a volume of a photopolymer.[15,16] The 2D light patterns act cumulatively to produce an optical 3D dose distribution that triggers polymerization of the irradiated material into the desired object. In the first conceptualization of volumetric additive manufacturing, simple objects were fabricated by irradiating a photopolymer reservoir with a superposition of multiple beams coming from fixed, predetermined orientations.[17] New volumetric printing processes, inspired by computed tomography (CT), enable the production of more complex objects by using 2D dynamic light fields.[15,16] Technical photopolymers such as acrylates[16] and elastomeric resins[15] have been printed, showing the ability to resolve features down to 80 µm.[15] However, the potential for regenerative medicine remains unexplored, and significant steps are required to further develop volumetric manufacturing into a cell printing technology.

In this work, we demonstrated the bioprinting of large living tissue constructs by processing cell-friendly hydrogel-based bioresins with a volumetric, visible light laser-based printer. In our setup, a 3D light dose distribution is deposited into a cylindrical container of photopolymer gel to permit its spatially selective crosslink (**Figure 1**A,B). To build up this 3D dose distribution, the resin container is set into rotation and synchronously irradiated with a sequence of 2D light patterns, computed by a Radon transform,[18] applying the principles of medical tomographic imaging in reverse. In other words, the light patterns represent projections of the object to fabricate along multiple rotational angles of the cylindrical volume of photopolymer. These dynamic light patterns are displayed into the build volume by irradiating a DLP modulator with a 405 nm laser source. Although each light pattern exposes the whole build volume, the light dose resulting from a single exposure is insufficient to crosslink the resin.[15] The polymer solidifies only in selective areas where the accumulation of multiple angular exposures results in an absorbed dose overcoming the gelation threshold (as exemplified in Video S1 and Figure S1, Supporting Information). As a consequence, and differently to the layerwise process of stereolithography, overcuring will always lead to off-target polymerization. Thus, identifying the minimum exposure time to gelate the 3D object within the optical field is paramount to optimize shape fidelity.

Several photoresponsive hydrogels have shown remarkable compatibility for cell encapsulation. Among them, gelatin methacryloyl (gelMA) has rapidly become a widely used and versatile bioink, for both extrusion-based and light-based fabrication.[19–22] Therefore, as a cell-friendly bioresin for volumetric printing, we designed a formulation based on gelMA dissolved in phosphate buffered saline (PBS), with lithium phenyl-2,4,6-trimethylbenzoyl-phosphinate (LAP) as photoinitiator for the free-radical polymerization of the methacryloyl moieties (gelRESIN). With this approach, complex, free-form structures could be generated within seconds from a volume of cell-laden hydrogels (Figure 1C). The chosen photoinitiator, LAP, exhibits

a superior quantum efficiency and molar extinction coefficient at visible wavelength (ε = 50 M^{-1} cm^{-1} at 405 nm), compared with other initiators used so far for the volumetric printing of noncell-compatible resins.[15] Importantly, in volumetric printing, the whole build volume must be addressed by each light pattern for the object reconstruction to be accurate. This feature sets an upper limit on the photoinitiator concentration. In other words, when designing a resin composition for volumetric printing, the initiator concentration must be low enough for the light to penetrate through the whole volume, but high enough to allow the gel to polymerize. To achieve that, a light intensity value corresponding to at least 37% of the incoming light intensity to reach the opposite edge of the build volume was found to be sufficient (**Figure 2**A). Using the Beer–Lambert law, this is equivalent to $\ln(10)\varepsilon Dc = 1$, where ε is the photoinitiator molar extinction coefficient (M^{-1} m^{-1}), D (m) is the diameter of the cylindrical build volume diameter, and c the photoinitiator concentration (mol m^{-3}). Interestingly, the LAP concentration required to produce well-defined printed structures was only 0.037% wt, a value considerably lower than what has commonly been used in previously reported additive bioprinting studies.[23–26] This reduces the potential toxicity risks that are correlated with high concentrations of this photoinitiator.[27,28]

First of all, VBP showed a promising volume accuracy, with printed human auricle models showing a volume variation of 5.71 ± 2.31%, when comparing the printed constructs acquired via microcomputed tomography (µCT) and the original STL files. Remarkably, and in contrast to other additive bioprinting approaches, printing time is not bound to the dimensions of the construct. To quantify and compare the printing time, we printed an anatomical human auricle model that was first miniaturized (volume ≈ 0.15 cm^3), then scaled two and three times (volume ≈ 1.23 and 4.14 cm^3, respectively). All VBP-printed models were fabricated within the same printing time (22.7 s). In extrusion-based bioprinting, the printing time increases cubically with the scaling factor, quickly reaching an unfavorable magnitude (>1–2 h) when cell-laden centimeter-scale objects are required without greatly compromising on resolution. Instead, in DLP processes (but not in conventional SLA), the printing time increases linearly as a function of the height of the construct, independently on the area to be printed in each individual layer (Figure 2B).[29] DLP processes can be accelerated by reducing the lifting time of each printed layer, as shown by the recent development of the continuous liquid interface printing (CLIP) method.[30] However, as calculated using our biocompatible gelRESIN, even when reducing the lifting time to zero, the overall fabrication time (10 s/layer with gelRESIN) would be one order of magnitude higher than that achieved with volumetric bioprinting (data not shown). Conversely, in volumetric bioprinting, the printing time can be consistently found in the range of tens of seconds, regardless of the volume of the construct, as long as the same irradiation intensity is supplied to the photopolymer. For example, to keep a constant printing time for a build volume scaled twice in each dimension, a laser output four times as powerful as that used for the unscaled volume is necessary. Furthermore, volumetric bioprinting results in seemingly artifact-free surface features, as illustrated by the smooth profile of the generated structures, including the printed auricle (Figure 2Ci, further discussion provided in the Supporting Information). These volumetric printed parts reflect the nature of the digital model and reproduce its surface features more faithfully, especially when compared with additive technologies. In fact, extrusion-based and DLP bioprinting exhibit a typical filament- and voxel-riddled pattern, respectively, that introduce an artifactual surface roughness profile in the construct (Figure 2Cii,iii). The resolution of volumetric printing is limited by optical and chemical phenomena. The optical resolution of volumetric printing is determined by the effective pixel size of the projected images at the center of the build volume, along with the depth of focus which determines to what degree the optical resolution is maintained at the edge of the build volume. The effective pixel size is 22.8 µm in our experiments, and with the current optics the resolution at the edge of the volume is 33 µm. A number of effects, such as the diffusion of chemical species, can decrease the resolution of volumetric printing methods,[16] and steps to maximize resolution have been recently described.[31]

Moreover, we demonstrated the possibility, unique to volumetric bioprinting, to print free-floating parts without the need for sacrificial support materials or two-photon polymerization approaches. This feature is paramount to generate systems able to reversibly modify their shape postprinting, and similar free-moving parts could be included also in structures printed with stimuli-responsive materials (often used in 4D printing),[32] for instance, to facilitate shape changes. Hydrogel-based actuators are prevalently obtained by exploiting the swelling capability of hydrogels in response to osmolarity, temperature, and pH,[32,33] and by endowing the materials with, that is, magnetic or electrical stimuli-responsive properties, for instance, by introducing nanoparticles within the hydrogel bulk.[7,34] On the other hand, the freedom of design provided by volumetric bioprinting approaches permits the production of such actuators through the direct fabrication of movable or articulating parts. To confirm this, we printed a fluidic valve inspired by the ball-and-cage cardiac valve prosthesis[35] (Figure 2Di–iii). Such a model, unlike other valve designs such as the anatomically inspired bi- and tri-leaflets,[26] cannot be directly fabricated by extrusion or DLP/DMD technologies in the absence of sacrificial supports. When connected to a fluidic system, the valve could function correctly, enabling unidirectional flow within the circuit (Figure 2Div,v, Videos S2 and S3, Supporting Information). This feature that can have potential applications in hydrogel-based microfluidics[26] or in hydrodynamic-actuated soft robots.[36] To achieve this type of complex constructs, the thermoreversible gelation of gelRESIN is particularly advantageous. In fact, printing in the gel state (at room temperature) is beneficial not only to prevent cell sedimentation during the fabrication step (Figure S2, Supporting Information) but also to provide positional stability to the construct, avoiding movement of printed parts due to potential changes in buoyancy post-crosslinking or due to the rotation of the photopolymer reservoir. Furthermore, experimental analysis of the cell sedimentation time prior to the thermal gelation revealed that cells are homogenously distributed throughout 2 cm thick hydrogel volumes, even if the reversible gelation is triggered after 10 min after cell mixing. This result also suggests that, given the rapidity of the VBP process, homogenous cell suspension could be achieved even when processing alternative bioresins that lack the thermal gelation

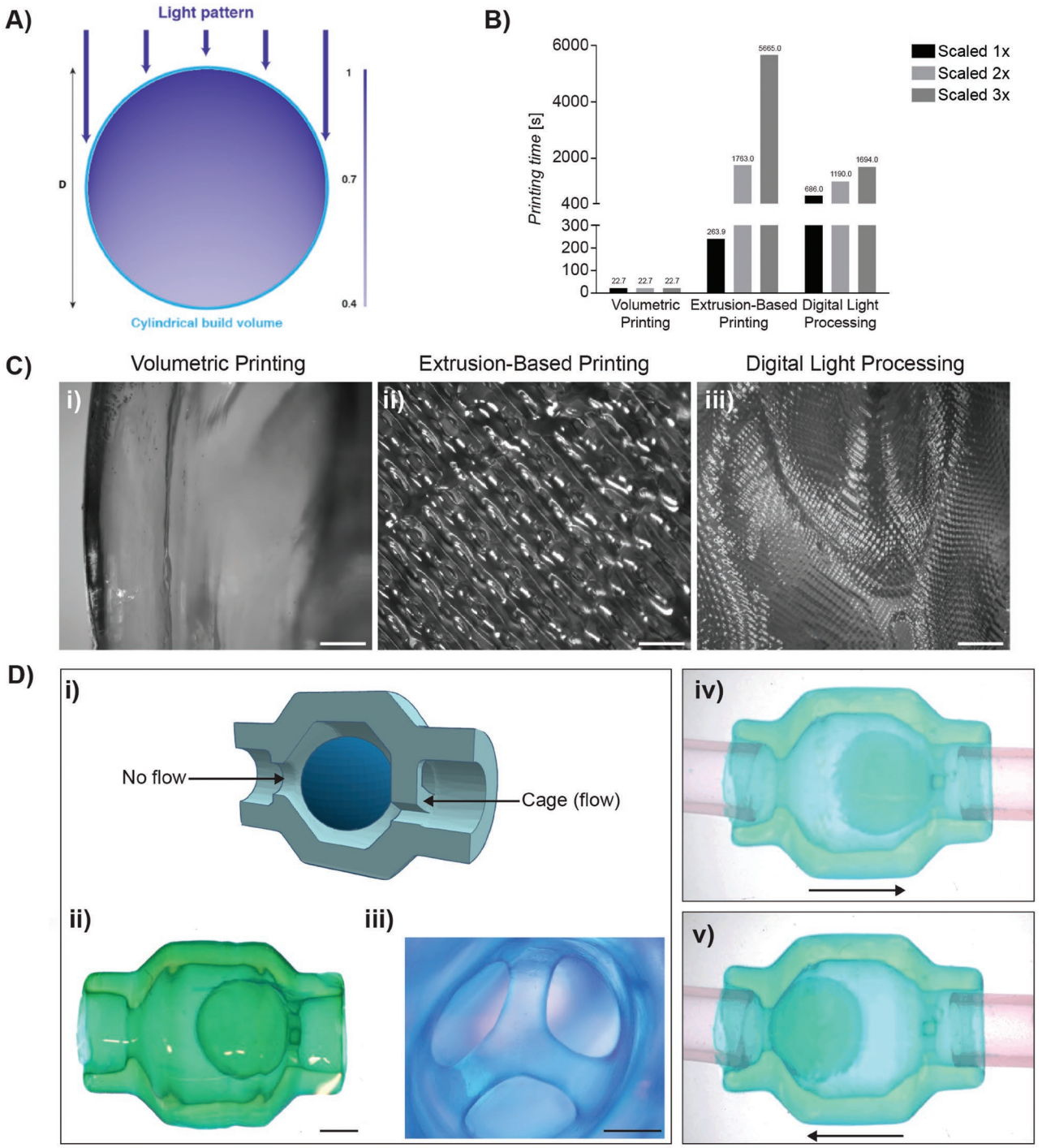

Figure 2. Main volumetric printing process parameters and printed construct features. A) Graphical representation of the light penetration pattern through the entire build volume in the presence of a photoinitiator. B) Fabrication time for the human auricle model scaled 1× (0.15 cm^3), 2× (1.23 cm^3), and 3× (4.14 cm^3) using different bioprinting techniques: volumetric printing, extrusion-based (bio)printing, and digital light processing. C) Close-up images of the surface features of the auricle fabricated through (i) volumetric printing, (ii) extrusion-based printing, and (iii) digital light processing (scale bars = 500 µm). D) Volumetric printing of a fluidic ball-cage valve with free-floating elements from a (i) computer-generated 3D model of the valve. (ii) Top view of the printed valve (scale bar = 2 mm), (iii) close-up of the cage segment that permits flow (scale bar = 1 mm), and video stills showing unidirectional flow functionality with an (iv) open and a (v) closed valve (black arrow represents the flow direction).

behavior of gelatin. Finally, after the material is selectively crosslinked, the unreacted hydrogel precursor is easily washed away in PBS or aqueous media at 37 °C, and the printed object is postcured, giving rise to a complete polymerization comparable to that of cast gelMA gels, as documented by the low sol fraction (Table S1, Supporting Information).

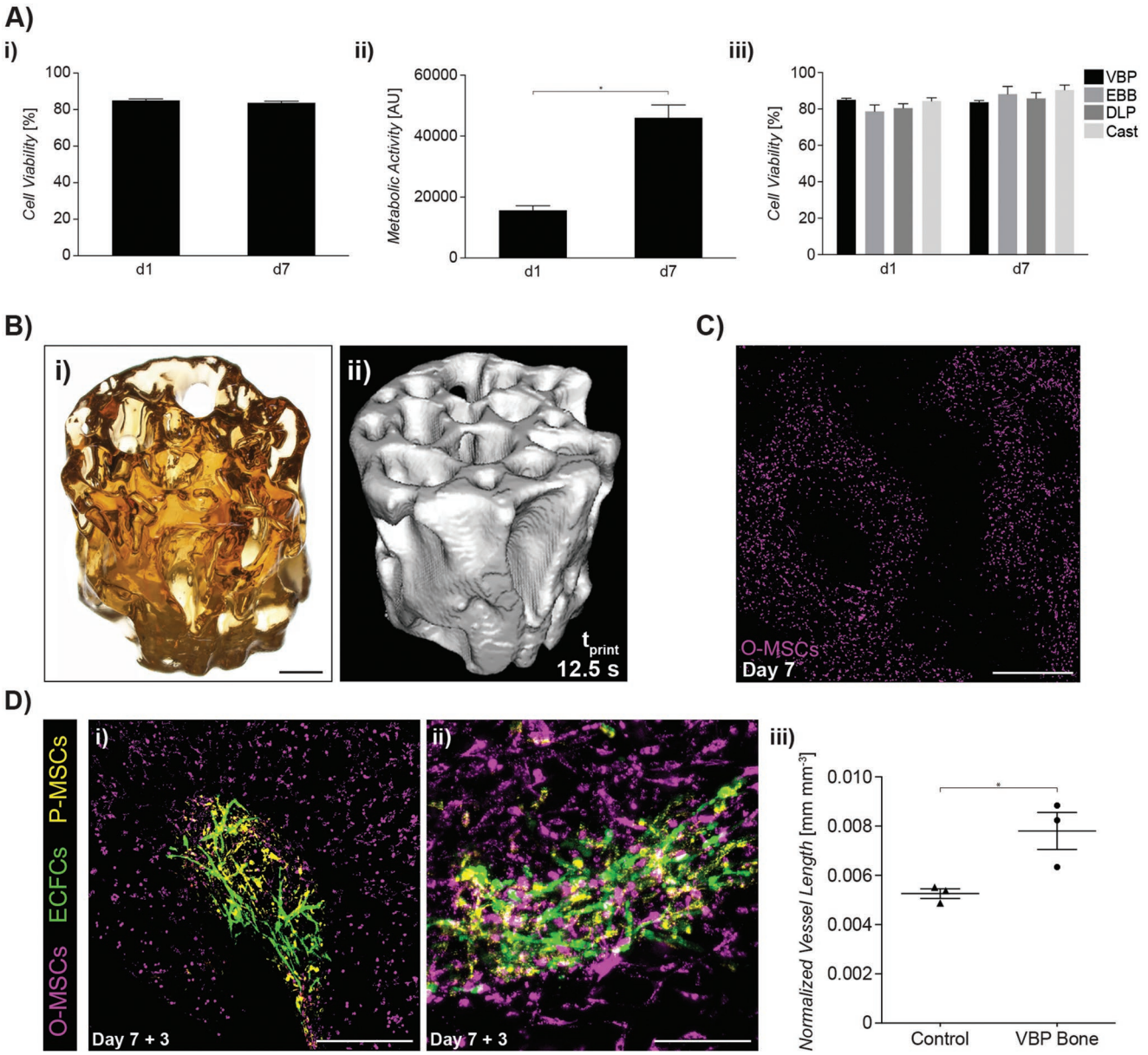

Figure 3. A) Volumetric bioprinted, ACPC-laden gelRESIN disc-shaped constructs were cultured for 7 d and exhibited (i) high cell viability (>85%), (ii) increased metabolic activity over time, and (iii) comparable cell survival compared to hydrogel casting and other commonly used bioprinting techniques: extrusion-based bioprinting and digital light processing. B) A complex trabecular bone model was fabricated to examine the development of salient characteristics post-printing. (i) The printed bone exhibited a porosity that extended throughout the extended 3D construct (scale bar = 2 mm), (ii) as shown through µCT imaging. C) The O-MSC-laden (pink) bone construct was cultured for 7 d (scale bar = 1 mm). D) Constructs were then seeded with ECFCs (green) and P-MSCs (yellow) to induce capillary formation. (i) ECFCs were shown to interconnect after three additional days of culture, filling the pores of the printed construct (scale bar = 500 µm), (ii) and were also shown to begin invading the bone compartment of the construct (scale bar = 250 µm). (iii) Vessel interconnectivity and length were also measured quantitatively and compared to a control 2D culture condition.

Notably, we demonstrated that living tissue constructs can be safely generated via volumetric bioprinting of gelRESIN without impacting cell survival. Structures with high cell viability (>85% postprinting, **Figure 3**Ai) were created, with cells showing an increase in metabolic activity over time (Figure 3Aii). Chondroprogenitor cell viability was preserved at high levels across 7 d of additional culture, with values comparable to those found for conventional hydrogel casting and other well-known bioprinting methods (no statistically significant differences, Figure 3Aiii). This result is also in line with several reports on safe and cytocompatible windows for radical-induced photopolymerization.[37–39] Additionally, as a nozzle-free method, volumetric bioprinting shows no risk of shear stress-induced cell damage or phenotype alteration which could compromise the function of the biological construct postprinting, as previously reported for certain high-viscosity bioinks for extrusion-based and inkjet printing.[13,40,41]

Further building on these results, an anatomical trabecular bone model laden with mesenchymal stromal cells (MSCs) was bioprinted using a μCT scan of a bone explant as a blueprint (cylindrical construct, 8.5 × 9.3 mm, Figure 3Bi,ii, Videos S4 and S5, Supporting Information). Generation of the trabecular architecture and the convoluted, interconnected porous network, goes beyond what can be created with conventional extrusion-based bioprinting. Using the volumetric printing approach, these structures were successfully reproduced with the smallest resolved feature measuring 144.69 ± 13.55 μm (Figure S3, Supporting Information). Likewise, we also showed the creation of fully perfusable hollow channels with an inner diameter of 200 μm (Figure S4, Supporting Information). Overall, current resolution is comparable with the most accurate extrusion-based technologies, and has the potential to be further improved, as already demonstrated with conventional resins.[15]

In biofabrication, the printing of an accurate 3D architecture is only the first step of many. In order to enable postprinting tissue maturation (either in vitro or in vivo), cells need to retain high viability, differentiation capacity, and the ability to synthesize bioactive compounds and interact with other cells in their surroundings. After volumetric bioprinting, cells could be maintained in culture, and the expression of salient physiological functions was observed over time (Figure 3C,D). More specifically, MSCs within the printed trabecular bone model were successfully primed in osteogenic medium for 7 d, as mimic of the osteoblasts within native bone (O-MSCs) (Figure 3C). These generated structures also allowed for further top-down tissue engineering strategies. In this case, the complex porous network of the cell-laden trabecular model could also be seeded with additional cells postprinting. For this, we delivered endothelial colony forming cells (ECFCs) and MSCs into the pore network between the printed O-MSC-laden trabeculae to generate a heterocellular structure. A coculture of osteogenically differentiating cells, vascular endothelial cells, and supporting MSCs that act as pericytes (P-MSCs) was successfully generated. After 3 d of culture, the formation of early angiogenic sprouts, typical of blood capillary network precursors,[42] was observed. Additionally, the introduced P-MSCs coaligned along these nascent ECFCs sprouts (Figure 3Di,ii, Videos S6 and S7, Supporting Information), suggesting a pericyte-like supporting activity.[42] Importantly, the density of such networks of organized sprouts, relative to the available volume within the pores of the model, was higher than that of precapillary networks generated by control cocultures of ECFCs and MSCs, when the bioprinted O-MSCs structure is not present (Figure 3Diii, Figure S5, Supporting Information). This phenomenon, together with the observation that these early capillaries began to invade the bone hydrogel matrix, suggests that the bioprinted O-MSCs have the ability to provide paracrine signals that promote the angiogenic process driven by ECFCs. These findings further support the notion that volumetric bioprinting allows for the realization of key cellular functions.

In order to facilitate the synthesis of new tissue matrix and its homogeneous distribution within a 3D hydrogel for regenerative medicine and tissue engineering applications, (bio)fabrication processes need to allow for the processing of high cell densities. While the described volumetric bioprinting approach can meet this requirement, inkjet- and extrusion-based processes present a greater challenge, due to the risk of nozzle clogging and nutrient depletion within the cartridge during extended printing times.[43] Furthermore, the ability to process hydrogels in the gel state ensures prevention of sedimentation of embedded cells[44] and permits homogeneous cell distribution within the printed volume. To assess this potential and the ability of bioprinted cells to synthesize new-tissue matrix, a meniscus-shaped implant was printed from an anatomical scan (**Figure 4**A, Video S8, Supporting Information), encapsulating 10^7 articular chondroprogenitor cells (ACPCs) mL^{-1}. These multipotent cells showed increased metabolic activity over time (Figure 4B) and exhibited high cell viability throughout the bioprinted structure (Figure S6, Supporting Information). These meniscus-shaped constructs could be successfully maintained in culture for at least 28 d during which synthesis of neo-fibrocartilage matrix was observed (Figure 4C). Importantly, such neo-extracellular matrix (ECM) resulted in a functional increase of the mechanical properties of the meniscal graft, as measured by indentation. The compressive modulus increased from 24.63 ± 0.65 kPa immediately after the volumetric printing process, until reaching values in the range of 266.54 ± 4.49 kPa, comparable to native human fibrocartilage.[45] Newly synthesized glycosaminoglycans (GAGs) were distributed throughout the volume of the printed construct (Figure 4D). High amounts of collagen type I were also detected (Figure 4E), typical for the human menisci, as well as minor amounts of collagen type II (Figure 4F), analogue to the native tissue composition. To further promote the maturation of these constructs, which were cultured under static conditions, the use of dynamic loading systems or bioreactors could be of interest for future studies, for instance, to induce physiological collagen fiber alignment.[46]

In summary, the results reported herein highlight the potential of volumetric printing as a novel, powerful, and versatile biofabrication strategy. Its ability to rapidly create large, free-form cell-laden structures, can solve many of the key challenges in bioprinting and regenerative medicine. With dramatically reduced printing times compared to conventional bioprinting methods, obtaining high cell numbers to be loaded into the printer and produce constructs with high cell density remain open challenges toward the fabrication of clinically relevant grafts. This could potentially be tackled with the use of novel sources of adult stem cells,[47] as well as with further refinement of induced pluripotent stem cell (iPSC) technology,[48,49] or of bioreactors for upscaling the production of regeneration-competent cells.[48,50]

Additionally, with the adoption of volumetric bioprinting in the field of biofabrication, several future developments can be expected. Here, we selected gelMA as a resin due to its well-established use in biofabrication approaches. However, there is virtually no limitation on the use of different photopolymers, and several photoresponsive natural or synthetic hydrogels could be optimized for this process (including but not limited to materials based on hyaluronan, PEG, alginate, or decellularized ECM) or even stimuli-responsive biomaterials for remote stimulation of the construct or controlled patterning of bioactive molecules.[51] Photochemistries alternative to methacryloyl addition polymerization could be employed as well, for instance, thiol–ene step growth polymerization as used in DLP

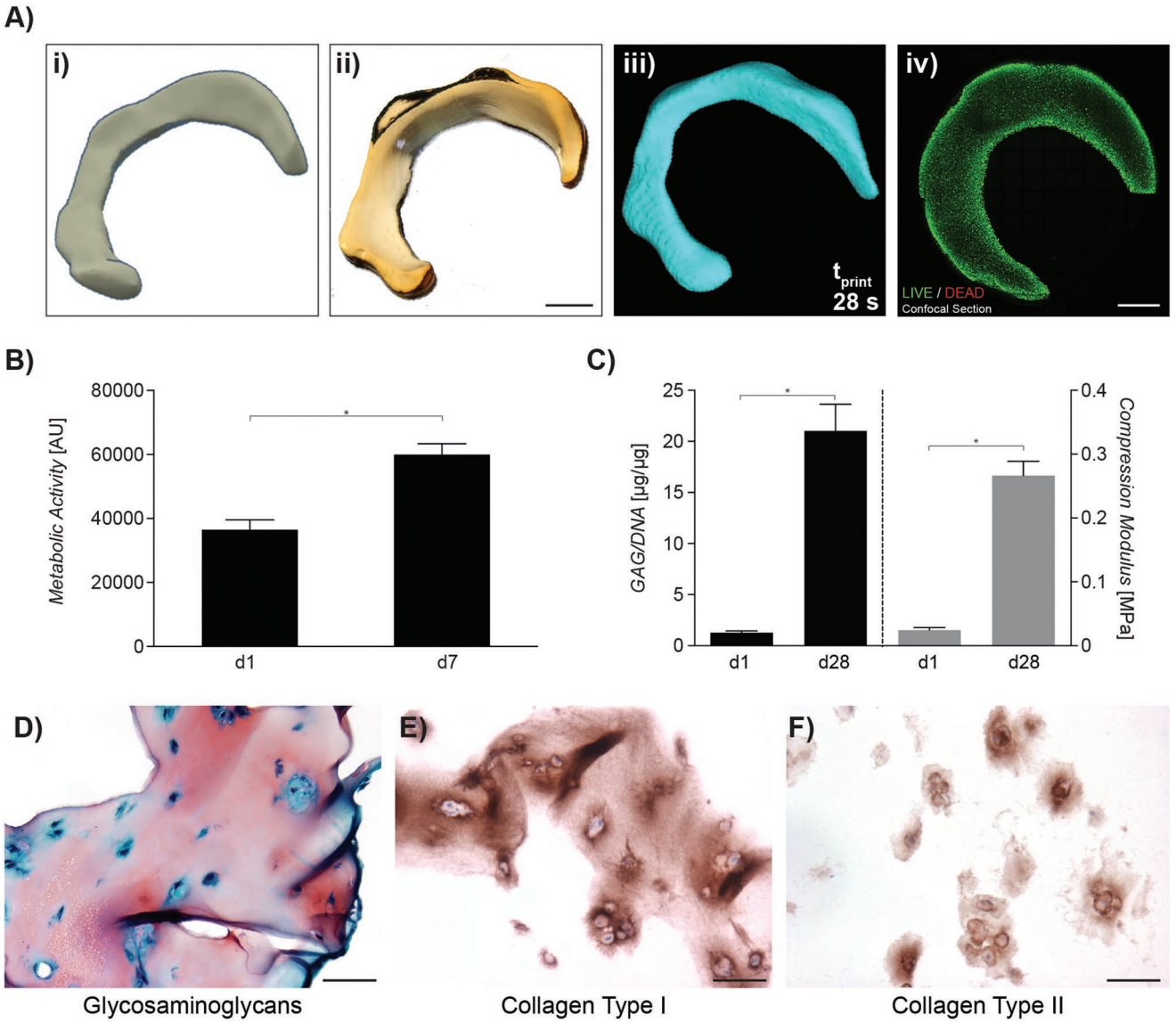

Figure 4. Long-term culture of meniscus-shaped, volumetric bioprinted constructs to assess matrix synthesis and neotissue formation. A) Meniscus constructs were printed from a (i) computer-generated 3D model and (ii) the resulting gelRESIN samples were cultured in vitro for 28 d (scale bars = 2 mm). (iii) The 3D structure of the printed menisci was assessed through µCT, and (iv) high cell viability throughout the construct was observed over a 7 d period. B) Metabolic activity increased over a 7 d evaluation period. C) In terms of neotissue formation, the bioprinted constructs exhibited a significant increase in glycosaminiglycan production, as well as an increase of the meniscus compressive modulus over a 28 d culture period. Matrix components present in the native meniscus were shown to be present throughout the bioprinted constructs: D) glycosaminoglycans, E) extensive amounts of collagen type I, and F) lower amounts of collagen type II (scale bars (D)–(F) = 50 µm).

printing.[52] Next steps pertaining to the technology should introduce the potential for printing multiple materials within the same process, as this will be important to further mimic the heterogeneous composition of living tissues. For example, multimaterial volumetric printing could be used to address the zonal architecture of certain tissues (i.e., cartilage, menisci), create cell and material gradients, replicate biological interfaces, introduce vascularization in a single step, or even coprint mechanically strong polymers to reinforce the cell-laden bioprinted hydrogels. The rapid speed of volumetric bioprinting is an important benefit for the production of tissues and disease models. The generation of large constructs with arbitrary shape can aid patient-specific regenerative medicine, in light of potential translation of clinically relevant grafts. At the same time, drug discovery and testing typically requires testing of a large number of molecule combinations on identical models, which can easily be produced on a large scale with the proposed method, also reducing costs related to personnel and machine time necessary per constructs. It is hoped that this capability can complement and even reduce animal testing in the intermediate phases of drug development, leading to lower development costs and fewer ethical issues. Complemented by these perspectives for future developments, our results and the volumetric bioprinting technology proposed herein pave the way for

the next generation of large and functional biofabricated grafts, with a wide array of envisioned applications for tissue regeneration, in vitro tissue and disease models, and soft robotics.

Experimental Section

Materials: gelMA (80% DoF) was synthesized as previously described and used as a 10% w/v solution in PBS.[53] As photoinitiator, lithium phenyl(2,4,6-trimethylbenzoyl)phosphinate (LAP, Tokyo Chemical Industry, Japan) was dissolved in PBS at 0.037% (w/v) in the hydrogel to induce a photocrosslinking reaction. In cast gelMA controls, LAP was dissolved at 0.2% w/v. Post-photocrosslinking of printed samples was carried out in a solution containing tris(2,2- bipyridyl) dichlororuthenium(II) hexahydrate (Ru, 0.5×10^{-3} M, Alfa Aesar, Germany) and sodium persulfate (SPS, 5×10^{-3} M, Sigma Aldrich, The Netherlands).

Volumetric Printing Procedure: To achieve volumetric bioprinting, six 405 nm laser diodes D with a 6.4 W combined power (HL40033G, Ushio, Japan) were collimated and coupled by lenses L1, L2, and L3 (L1: f = 3.1 mm aspheric lens; L2: f = 200 mm lens; L3: 3.1 mm aspheric lens) in a square fiber F as illustrated in Figure S7 (Supporting Information). The output of the fiber was then magnified and projected onto a digital micromirror device (DMD) via an aspheric lens and a set of orthogonal cylindrical lenses C1 and C2 (C1: f = 250 mm cylindrical lens; C2: f = 300 mm cylindrical lens). The surface of the DMD was imaged via a 4f-system (L5: f = 150 mm lens and L6: f = 250 mm lens) into a Ø16.75 mm cylindrical glass vial (V) containing the photopolymer (PR). In the Fourier plane of the afocal system, an aperture (A) blocks the unwanted diffraction orders from the DMD. To address the largest build volume possible, the glass vial V was immersed into a vat (VAT) containing a liquid matching the refractive index of the resin (in this study, water). Hence, the addressable volume inside the photopolymer is approximately 14 mm × 14 mm × 20 mm. A feedback system was integrated in the volumetric printing setup by taking advantage of the transparency of the build volume. As shown in Figure S6 (Supporting Information), a 671 nm laser (LAS; MLS-671-FN, CNI, China) was expanded by an afocal system (lenses L7 and L8) to match the build volume section. The build volume was subsequently imaged by a camera (CAM). The photoinitiators used in this study are not sensitive to the 671 nm imaging wavelength and this feedback system does not impact the printing parameters. The light patterns displayed during the volumetric printing process were calculated using a filtered back-projection algorithm,[15] as further detailed in the Supporting Information.

Sample Processing Postvolumetric Printing: Vials containing the printed constructs were heated to 37 °C to melt the unpolymerized gelRESIN, and samples were washed with prewarmed PBS, followed by 2.5 min of additional crosslinking in a Ru/SPS bath in PBS, under a visible light handheld lamp (130 lumen, Ansmann, Germany). Due to the transparency of the constructs printed with LAP, the Ru/SPS crosslinking system was chosen as it induces an orange staining of the hydrogels, thus facilitating their visualization, and is compatible to ensure homogenous crosslinking throughout large-scale printed constructs (Figure S8, Supporting Information).[54]

Cell Isolation and Culture: Equine tissue samples and cells were obtained from deceased horse donors, donated to science by their owner and according to the guidelines of the Institutional Animal Ethical Committee. Equine-derived ACPCs and bone marrow-derived MSCs were isolated as previously described.[55] The procedures to isolate human tissue and cells were approved by the research ethics committee of the University Medical Center Utrecht. Human MSCs were isolated from bone marrow aspirates obtained from consenting patients as previously described.[42] ECFCs were isolated from human cord blood (procedure was approved by the medical research ethics committee, University Medical Center Utrecht, informed consent was obtained from the mothers).[42] Details of the culture media are reported in the Supporting Information.

Viability in Volumetric Bioprinting: ACPCs were harvested at passage 3, embedded in gelRESIN at a density of 10^7 cells mL^{-1}, and printed into disc constructs (1 mm height × 5 mm diameter). These were cultured for 7 d in ACPC expansion medium, which was refreshed twice per week. Metabolic activity was measured with a resazurin assay (resazurin sodium salt, Alfa Aesar, Germany) and cell viability was evaluated using a LIVE/DEAD assay (Calcein, ethidium homodimer, Thermo Fischer Scientific, The Netherlands) after 1 and 7 d ($n = 5$).

Stereomicroscopy and Computed Tomography: Macroscopic images were acquired using an Olympus SZ61 stereomicroscope coupled with an Olympus DP70 digital camera (Olympus Soft Imaging Solutions GmbH, The Netherlands). µCT scans were performed using a contrast agent (CA4+, MW = 1354 g mol^{-1}, $q = +4$) that was synthesized and kindly provided by the lab of Mark W. Grinstaff.[56] Printed constructs were incubated in a solution containing 10 mgI mL^{-1} CA4+ in PBS for 3 h, washed and briefly dried with tissue paper, prior to being scanned with a Quantum FX µCT scanner (voxel size = 20 μm^3, 90 kV tube voltage, 200 µA tube current, and 3 min of scan time, Perkin Elmer, USA). The volume of the resulting scans ($n = 3$ independent prints) was calculated using the "volume fraction" function of the Bone J plugin for Image J (http://bonej.org).

Comparison between Different Bioprinting Technologies: A human auricle model was scaled 1×, 2×, and 3× its original volume, and printing time was compared with extrusion-based and lithography-based DLP bioprinting. For extrusion-based printing, gelRESIN was printed with a pneumatic-driven system (23G stainless steel nozzle, temperature = 18 °C, feed rate = 10 mm s^{-1}, pressure = 0.12 MPa, 3DDiscovery, regenHU, Switzerland). For DLP printing, gelRESIN was printed with DLP station (v5, Atum 3D, The Netherlands) equipped with a 405 nm projector (layer exposure time = 10 s, intensity = 15 mW cm^2). Although the printer permits a minimum resolution of 50 µm in the *Z*-direction, printing resolution was artificially worsened increasing the layer height to 300 µm, to match the resolution achievable with extrusion-based printing and greatly decrease the printing time. The surface profile of the constructs was assessed using the best available resolution and inks for extrusion and DLP printing enabling most accurate and defect-free prints. For extrusion printing, 40% w/v solution of Pluronic F-127 (Sigma Aldrich, The Netherlands) in PBS was printed (temperature = 21 °C, feed rate = 20 mm s^{-1}, pressure = 0.22 MPa). For DLP printing, a bioresin based on polyvinyl alcohol methacrylate (PVA-MA, 10% w/v in PBS), enabling resolution between 25 and 50 µm was used as previously described.[29]

Fluidic Experiments: The printed ball and cage valves were connected at both ends to silicone tubing with the same outer diameter to the inner diameter of the ends of the valve, and the flexibility of the tubing prevented leakage from the connection. Perfusion with PBS either pristine or supplemented with 10 mg mL^{-1} Cytodex 1 microbeads stained with Ponceau 4R to enhance visualization (diameter = 147–248 µm, GE Healthcare) was handled with a disposable syringe. Images and videos were taken with the aforementioned stereomicroscope.

Trabecular Bone Bioprinting and Culture: Equine-derived MSCs were harvested at passage 3, labeled with cell labeling solution DiD (Vybrant cell labeling kit, Thermo Fischer Scientific, The Netherlands, $\lambda_{ex} = 644$ nm, $\lambda_{em} = 665$ nm) and embedded in gelRESIN at a density of 1×10^6 cells mL^{-1}. Constructs were cultured for 7 d in osteogenic induction medium. Cell presence within the trabecular structures was imaged at day 7 via confocal laser scanning microscopy (SPX8, Leica Microsystems, The Netherlands). After this time, the pores of the bioprinted bone were seeded with human-derived ECFCs (passage 10) and P-MSCs (passage 4) labeled with green fluorescent protein (GFP)[57] and DiL (Vybrant cell labeling kit, $\lambda_{ex} = 549$ nm, $\lambda_{em} = 565$ nm), respectively. To enable the formation of 3D capillaries within the porosity of the bone construct, these cells were injected together with matrigel (Growth Factor Reduced, Corning, USA, 1:1 dilution in endothelial media) at a density of 4.5×10^6 MSCs and 1.25×10^6 ECFCs mL^{-1}. Loaded samples were cultured in endothelial medium for additional 3 d, to observe the onset of angiogenic sprouts formation via confocal

microscopy. The length of the angiogenic network formed by ECFCs was calculated using the Angiogenesis Analyzer plugin for ImageJ (http://image.bio.methods.free.fr/ImageJ/?Angiogenesis-Analyzer-for-ImageJ). Total length was normalized against the volume available for cell migration and sprouting. ECFCs and P-MSC seeded into 96 well plates in matrigel were used as controls.

Bioprinted Menisci and Neotissue Formation: ACPCs were harvested at passage 3, embedded in gelRESIN at a density of 10^7 cells mL^{-1}, and bioprinted into meniscus-shaped constructs. Samples were cultured for 28 d in chondrogenic differentiation medium, which was refreshed twice per week. Samples were analyzed for metabolic activity (resazurin assay) and cell viability using a LIVE/DEAD assay after 1 and 7 d of culture (n = 3). Fibrocartilage formation potential was assessed by quantifying GAG (dimethylmethylene blue assay, DMMB, Sigma Aldrich) and DNA (Picogreen Quant-iT, Thermo Fischer Scientific, The Netherlands) synthesis after 1 and 28 d of culture, as well as via Safranin-O, collagen I, and collagen II histological staining on paraffin-embedded samples (n = 3). Details of the immunohistochemical procedures are reported in the Supporting Information. Compressive properties of the printed menisci were probed in an indentation-based compression test, with a Dynamic Mechanical Analyzer (DMA Q800, TA Instruments, The Netherlands), equipped with a cylindrical flat piston (diameter = 2 mm). Samples at days 1 and 28 of culture were subjected to a force ramp 0.5 N min^{-1} (n = 3–4). The compression modulus was calculated as the slope of the stress/strain curve in the 10–15% strain range.

Statistics: Results were reported as mean ± standard error. Statistical analyses were performed using GraphPad Prism 7.0 (GraphPad Software, USA). For the quantitative data, single comparisons were assessed via a one or two-way ANOVA, followed by post hoc Bonferroni correction to test differences between groups. When normality could not be assumed, nonparametric tests were performed. For the blood vessel length analysis, the quantification of the GAG/DNA ratio, and the mechanical testing, a Mann–Whitney test was performed. Differences were found to be significant when $p < 0.05$.

Supporting Information

Supporting Information is available from the Wiley Online Library or from the author.

Acknowledgements

P.N.B., P.D., and D.L. contributed equally to this work. The authors would like to acknowledge Joao Garcia Marques for his support with the µCT imaging of the printed hydrogels, Chris van Dijk for the fruitful discussions on the vascularization assays, Dr. Debby Gawlitta and Iris Pennings for kindly providing the human ECFCs and MSCs, and Cody Fell and Mattie van Rijen for their help with the cell culture and the histological stainings. The authors would also like to acknowledge Lely Feletti and Prof. Aleksandra Radenovic (EPFL-LBEN) for facilitating the access to cell culture equipment, and Dr. Nikolaos Nianias (Readily3D) for the volumetric printing of the Dom Tower. P.N.B., J.M., and R.L. acknowledge the funding from the ReumaNederland (LLP-12 and LLP-22), the European Research Council (Grant Agreement No. 647426, 3DJOINT), and from the Horizon 2020 research and innovation program under the Grant Agreement No. 814444 (MEFISTO). R.L. also acknowledges the Materials-Driven Regeneration Young Talent Incentives Program for its financial support. P.D., D.L., and C.M. acknowledge the financial support of the Gebert Rüf Stiftung via the grant "Flexprint" (GRS-057/18, Pilot Projects track). P.D. and D.L. acknowledge the financial support of EPFL through the Innogrant 17-16 and the Enable grant for the "Holoprint" project. P.D. acknowledges the support of the SNSF and Innosuisse via the Bridge PoC grant 20B1-1_184178.

Conflict of Interest

The authors declare no conflict of interest.

Keywords

biofabrication, bioinks, bioresins, cell encapsulation, photopolymers, tomographic laser prototyping

Received: July 2, 2019
Revised: July 29, 2019
Published online:

[1] J. Crest, A. Diz-Muñoz, D.-Y. Chen, D. A. Fletcher, D. Bilder, *Elife* **2017**, *6*, e24958.
[2] H. Donnelly, M. Salmeron-Sanchez, M. J. Dalby, *J. R. Soc., Interface* **2018**, *15*, 20180388.
[3] J. A. Brassard, M. P. Lutolf, *Cell Stem Cell* **2019**, *24*, 860.
[4] N. Gjorevski, N. Sachs, A. Manfrin, S. Giger, M. E. Bragina, P. Ordóñez-Morán, H. Clevers, M. P. Lutolf, *Nature* **2016**, *539*, 560.
[5] S. A. Matarazzo, *PLoS One* **2015**, *10*, e0120436.
[6] G. Bahcecioglu, N. Hasirci, B. Bilgen, V. Hasirci, *Biofabrication* **2019**, *11*, 025002.
[7] R. Tognato, A. R. Armiento, V. Bonfrate, R. Levato, J. Malda, M. Alini, D. Eglin, G. Giancane, T. Serra, *Adv. Funct. Mater.* **2018**, *28*, 1804647.
[8] L. Moroni, T. Boland, J. A. Burdick, C. De Maria, B. Derby, G. Forgacs, J. Groll, Q. Li, J. Malda, V. A. Mironov, C. Mota, M. Nakamura, W. Shu, S. Takeuchi, T. B. F. Woodfield, T. Xu, J. J. Yoo, G. Vozzi, *Trends Biotechnol.* **2018**, *8*, 013001.
[9] H.-W. Kang, S. J. Lee, I. K. Ko, C. Kengla, J. J. Yoo, A. Atala, *Nat. Biotechnol.* **2016**, *34*, 312.
[10] M. M. Laronda, A. L. Rutz, S. Xiao, K. A. Whelan, F. E. Duncan, E. W. Roth, T. K. Woodruff, R. N. Shah, *Nat. Commun.* **2017**, *8*, 15261.
[11] E. A. Bulanova, E. V. Koudan, J. Degosserie, C. Heymans, F. D. A. S. Pereira, V. A. Parfenov, Y. Sun, Q. Wang, S. A. Akhmedova, I. K. Sviridova, N. S. Sergeeva, G. A. Frank, Y. D. Khesuani, C. E. Pierreux, V. A. Mironov, *Biofabrication* **2017**, *9*, 034105.
[12] M. de Ruijter, A. Ribeiro, I. Dokter, M. Castilho, J. Malda, *Adv. Healthcare Mater.* **2019**, *8*, 1800418.
[13] M. Müller, E. Öztürk, Ø. Arlov, P. Gatenholm, M. Zenobi-Wong, *Ann. Biomed. Eng.* **2017**, *45*, 210.
[14] J. K. Hohmann, M. Renner, E. H. Waller, G. von Freymann, *Adv. Opt. Mater.* **2015**, *3*, 1488.
[15] D. Loterie, P. Delrot, C. Moser, **2018**, https://doi.org/10.13140/RG.2.2.20027.46889.
[16] B. E. Kelly, I. Bhattacharya, H. Heidari, M. Shusteff, C. M. Spadaccini, H. K. Taylor, *Science* **2019**, *363*, 1075.
[17] M. Shusteff, A. E. M. Browar, B. E. Kelly, J. Henriksson, T. H. Weisgraber, R. M. Panas, N. X. Fang, C. M. Spadaccini, *Sci. Adv.* **2017**, *3*, eaao5496.
[18] A. C. Kak, M. Slaney, G. Wang, *Med. Phys.* **2002**, *29*, 107.
[19] A. K. Miri, D. Nieto, L. Iglesias, H. Goodarzi Hosseinabadi, S. Maharjan, G. U. Ruiz-Esparza, P. Khoshakhlagh, A. Manbachi, M. R. Dokmeci, S. Chen, S. R. Shin, Y. S. Zhang, A. Khademhosseini, *Adv. Mater.* **2018**, *30*, 1800242.
[20] B. J. Klotz, D. Gawlitta, A. J. W. P. Rosenberg, J. Malda, F. P. W. Melchels, *Trends Biotechnol.* **2016**, *34*, 394.
[21] G. L. Ying, N. Jiang, S. Maharjan, Y. X. Yin, R. R. Chai, X. Cao, J. Z. Yang, A. K. Miri, S. Hassan, Y. S. Zhang, *Adv. Mater.* **2018**, *30*, 1805460.

[22] L. Ouyang, J. A. Burdick, W. Sun, *ACS Appl. Mater. Interfaces* **2018**, *10*, 12424.
[23] L. Ouyang, C. B. Highley, W. Sun, J. A. Burdick, *Adv. Mater.* **2017**, *29*, 1604983.
[24] C. Xu, W. Lee, G. Dai, Y. Hong, *ACS Appl. Mater. Interfaces* **2018**, *10*, 9969.
[25] S. H. Kim, Y. K. Yeon, J. M. Lee, J. R. Chao, Y. J. Lee, Y. B. Seo, M. T. Sultan, O. J. Lee, J. S. Lee, S. I. Yoon, I. S. Hong, G. Khang, S. J. Lee, J. J. Yoo, C. H. Park, *Nat. Commun.* **2018**, *9*, 1620.
[26] B. Grigoryan, S. Paulsen, D. Corbett, D. Sazer, C. L. Fortin, A. Zaita, P. Greenfield, N. Calafat, J. Gounley, A. Ta, F. Johansson, A. Randles, J. J. Rosenkrantz, J. Louis-Rosenberg, P. Galie, K. Stevens, J. Miller, *Science* **2019**, *364*, 458.
[27] R. Holmes, X. B. Yang, A. Dunne, L. Florea, D. Wood, G. Tronci, *Polymers* **2017**, *9*, 226.
[28] L. A. Sawicki, A. M. Kloxin, *J. Vis. Exp.* **2016**, *115*, 54462.
[29] K. S. Lim, R. Levato, P. F. Costa, M. D. Castilho, C. R. Alcala-Orozco, K. M. A. Van Dorenmalen, F. P. W. Melchels, D. Gawlitta, G. J. Hooper, J. Malda, T. B. F. Woodfield, *Biofabrication* **2018**, *10*, 034101.
[30] J. R. Tumbleston, D. Shirvanyants, N. Ermoshkin, R. Janusziewicz, A. R. Johnson, D. Kelly, K. Chen, R. Pinschmidt, J. P. Rolland, A. Ermoshkin, E. T. Samulski, J. M. DeSimone, *Science* **2015**, *347*, 1349.
[31] D. Loterie, P. Delrot, C. Moser, **2019**, https://doi.org/10.13140/RG.2.2.35613.26082.
[32] A. Kirillova, R. Maxson, G. Stoychev, C. T. Gomillion, L. Ionov, *Adv. Mater.* **2017**, *29*, 1703443.
[33] S. Miao, H. Cui, M. Nowicki, L. Xia, X. Zhou, S. J. Lee, W. Zhu, K. Sarkar, Z. Zhang, L. G. Zhang, *Adv. Biosyst.* **2018**, *2*, 1800101.
[34] S. R. Shin, B. Migliori, B. Miccoli, Y. C. Li, P. Mostafalu, J. Seo, S. Mandla, A. Enrico, S. Antona, R. Sabarish, T. Zheng, L. Pirrami, K. Zhang, Y. S. Zhang, K. T. Wan, D. Demarchi, M. R. Dokmeci, A. Khademhosseini, *Adv. Mater.* **2018**, *30*, 1704189.
[35] W. Y. Lim, G. Lloyd, S. Bhattacharyya, *Heart* **2017**, *103*, 268.
[36] M. Wehner, R. L. Truby, D. J. Fitzgerald, B. Mosadegh, G. M. Whitesides, J. A. Lewis, R. J. Wood, *Nature* **2016**, *536*, 451.
[37] M. Bartnikowski, N. J. Bartnikowski, M. A. Woodruff, K. Schrobback, T. J. Klein, *Acta Biomater.* **2015**, *27*, 66.
[38] N. E. Fedorovich, M. H. Oudshoorn, D. van Geemen, W. E. Hennink, J. Alblas, W. J. A. Dhert, *Biomaterials* **2009**, *30*, 344.
[39] E. R. Ruskowitz, C. A. Deforest, *ACS Biomater. Sci. Eng.* **2019**, *5*, 2111.
[40] V. H. M. Mouser, R. Levato, A. Mensinga, W. J. A. Dhert, D. Gawlitta, J. Malda, *Connect. Tissue Res.* **2018**, https://doi.org/10.1080/03008207.2018.1553960.
[41] A. Blaeser, D. F. D. Campos, U. Puster, W. Richtering, M. M. Stevens, H. Fischer, *Adv. Healthcare Mater.* **2016**, *5*, 326.
[42] I. Pennings, L. A. van Dijk, J. van Huuksloot, J. O. Fledderus, K. Schepers, A. K. Braat, E. C. Hsiao, E. Barruet, B. M. Morales, M. C. Verhaar, A. J. W. P. Rosenberg, D. Gawlitta, *J. Tissue Eng. Regener. Med.* **2019**, *13*, 433.
[43] B. Lorber, W. K. Hsiao, I. M. Hutchings, K. R. Martin, *Biofabrication* **2014**, *6*, 015001.
[44] V. Chan, P. Zorlutuna, J. H. Jeong, H. Kong, R. Bashir, *Lab Chip* **2010**, *10*, 2062.
[45] A. J. Almarza, K. A. Athanasiou, *Ann. Biomed. Eng.* **2004**, *32*, 2.
[46] J. L. Puetzer, L. J. Bonassar, *Tissue Eng., Part A* **2016**, *22*, 907.
[47] C. K. F. Chan, G. S. Gulati, R. Sinha, J. V. Tompkins, M. Lopez, A. C. Carter, R. C. Ransom, A. Reinisch, T. Wearda, M. Murphy, R. E. Brewer, L. S. Koepke, O. Marecic, A. Manjunath, E. Y. Seo, T. Leavitt, W. J. Lu, A. Nguyen, S. D. Conley, A. Salhotra, T. H. Ambrosi, M. R. Borrelli, T. Siebel, K. Chan, K. Schallmoser, J. Seita, D. Sahoo, H. Goodnough, J. Bishop, M. Gardner, R. Majeti, D. C. Wan, S. Goodman, I. L. Weissman, H. Y. Chang, M. T. Longaker, *Cell* **2018**, *175*, 43.
[48] S. Greuel, G. Hanci, M. Böhme, T. Miki, F. Schubert, M. Sittinger, C. Mandenius, K. Zeilinger, N. Freyer, *Cell Prolif.* **2019**, *52*, e12604.
[49] U. Martin, *Adv. Drug Delivery Rev.* **2017**, *120*, 108.
[50] R. Levato, J. Visser, J. A. Planell, E. Engel, J. Malda, M. A. Mateos-Timoneda, *Biofabrication* **2014**, *6*, 035020.
[51] J. A. Shadish, G. M. Benuska, C. A. DeForest, *Nat. Mater.* **2019**, https://doi.org/10.1038/s41563-019-0367-7.
[52] S. Bertlein, G. Brown, K. S. Lim, T. Jungst, T. Boeck, T. Blunk, J. Tessmar, G. J. Hooper, T. B. F. Woodfield, J. Groll, *Adv. Mater.* **2017**, *29*, 1703404.
[53] F. P. W. Melchels, M. M. Blokzijl, R. Levato, Q. C. Peiffer, M. de Ruijter, W. E. Hennink, T. Vermonden, J. Malda, *Biofabrication* **2016**, *8*, 035004.
[54] K. S. Lim, B. J. Klotz, G. C. J. Lindberg, F. P. W. Melchels, G. J. Hooper, J. Malda, D. Gawlitta, T. B. F. Woodfield, *Macromol. Biosci.* **2019**, *19*, 1900098.
[55] R. Levato, W. R. Webb, I. A. Otto, A. Mensinga, Y. Zhang, M. van Rijen, R. van Weeren, I. M. Khan, J. Malda, *Acta Biomater.* **2017**, *61*, 41.
[56] R. C. Stewart, A. N. Patwa, H. Lusic, J. D. Freedman, M. Wathier, B. D. Snyder, A. Guermazi, M. W. Grinstaff, *J. Med. Chem.* **2017**, *60*, 5543.
[57] B. J. Klotz, K. S. Lim, Y. X. Chang, B. G. Soliman, I. Pennings, F. P. W. Melchels, T. B. F. Woodfield, A. J. W. P. Rosenberg, J. Malda, D. Gawlitta, *Eur. Cells Mater.* **2018**, *35*, 335.